NASA
Technical Memorandum 105388

AVSCOM
Technical Report 90-C-029

Contact Stresses in Meshing Spur Gear Teeth: Use of an Incremental Finite Element Procedure

Chih-Ming Hsieh and Ronald L. Huston
University of Cincinnati
Cincinnati, Ohio

and

Fred B. Oswald
Lewis Research Center
Cleveland, Ohio

March 1992

NASA

US ARMY
AVIATION
SYSTEMS COMMAND

CONTACT STRESSES IN MESHING SPUR GEAR TEETH: USE OF AN INCREMENTAL FINITE ELEMENT PROCEDURE

Chih-Ming Hsieh* and Ronald L. Huston
University of Cincinnati
Cincinnati, Ohio 45221-0072

and

Fred B. Oswald
National Aeronautics and Space Administration
Lewis Research Center
Cleveland, Ohio 44135-3191

E-6776

SUMMARY

Contact stresses in meshing spur gear teeth are examined. The analysis is based upon an incremental finite element procedure that simultaneously determines the stresses in and the contact region between the meshing teeth. The teeth themselves are modeled by two-dimensional plane strain elements. Friction effects are included, with the friction forces assumed to obey Coulomb's law. The analysis also assumes that the displacements are small and that the tooth materials are linearly elastic. The analysis procedure is validated by comparing its results with those for the classical case of two contacting semicylinders obtained from the Hertz method. Agreement is excellent.

INTRODUCTION

The life and performance of gear teeth are directly related to the ability of the teeth to withstand contact stresses. Contact stresses may produce pitting within the contact area and eventually lead to tooth failure. In spite of the importance of contact stresses in gears, comprehensive analyses of these stresses have not been extensively reported in the literature. Indeed, most analyses are based upon procedures that require simplified assumptions about the geometry of the contacting surfaces. Although these assumptions are needed for the classical procedures, their use raises questions about the accuracy and applicability of the results.

In this report we attempt to obtain a more representative and hence a more accurate analysis. The method is based upon an incremental finite element procedure (an iterative technique) that simultaneously determines the stresses and the contact area. Our motivation for using the finite element method (FEM) is based upon the success of the method in determining fillet stresses due to gear tooth bending (refs. 1 and 2). Our motivation for using the incremental procedure is based upon the success of other analysts in using it with contact analyses. For example, in 1970 Wilson and Parsons (ref. 3) used a differential displacement method to study frictionless contact problems. This approach was later extended by Ohte (ref. 4) to include frictional effects. In 1979 Okamoto and Nakazawa (ref. 5) presented the incrementation technique. This technique was also presented at about the same time by Skinner and Streiner (ref. 6) and by Urzua et al. (ref. 7). The technique was presented in automated form by Torstenfelt in 1984 (ref. 8).

---

*Chih-Ming Hsieh is presently at Modern Engineering, Warren, Michigan 48092.

The incremental procedure enjoys a number of advantages over more traditional finite element procedures: Specifically, (1) no special elements, such as gap elements or contact elements, are needed; (2) the calculated incremental loads follow the actual load history; (3) friction forces , once computed, are treated as known tangential loads and thus the standard analysis procedures of the finite element method remain intact; and (4) general-purpose finite element codes may readily be used in the analysis. In the research described herein we apply the incremental finite element procedure to the special geometry of involute spur gear teeth. The balance of this report presents the basic formulation of the method, the automation of the method, a validation of the method, some results for spur gear contact stresses, and a discussion and some concluding remarks.

SYMBOLS

a	semilength of contact
E	elastic modulus
e	accuracy parameter
F	nodal force in contact region
$\{F\}$	column vector of nodal global forces
$\{\Delta F\}$	incremental global force vector
[I]	identity submatrix
[K]	global stiffness matrix
n	normal unit vector in contact region
P(x)	pressure as function of x
p_0	maximum normal contact pressure
R	nodal reaction force in contact region
$\{\Delta R\}$	incremental nodal load vector
[S],[Q]	nonsquare transformation matrices
[T]	transformation matrix
t	tangential unit vector in contact region
U	nodal displacement in contact region
$\{U\}$	column vector of nodal global displacements
$\{\Delta U\}$	incremental global displacement vector
$\alpha_1,\alpha_2,\alpha_3$	scale factors defined in equations (17), (18), and (20)
δ	gap distance
$\{\delta_n\}$	nodal separation in contact region
μ	coefficient of friction between contacting bodies
ν	Poisson's ratio
σ_x,σ_y	normal stresses

τ shear stress

Subscripts and symbols:

a,b refers to bodies a and b

i,i′ typical pair of contacting nodes

max maximum

n,t normal and tangential directions

$\hat{}$ represents matrix in local (n,t) coordinate system

METHOD FORMULATION

The incremental procedure is an application and natural extension of the basic finite element method: Let the governing matrix equation for a finite element analysis be written as

$$\{F\} = [K]\{U\} \tag{1}$$

where $\{F\}$ is the column vector of nodal global forces, $[K]$ is the global stiffness matrix, and $\{U\}$ is the column vector of nodal global displacements.

Consider a structure discretized into elements and nodes such that equation (1) relates the nodal global forces and displacements. Let there be an increment in the nodal forces. Let these incremental forces be designated by the column vector $\{\Delta F\}$, and let the resulting incremental nodal global displacements be designated by the vector $\{\Delta U\}$. If the global geometry of the structure is essentially unchanged by the force increment, the global stiffness matrix $[K]$ is essentially unchanged. Hence, from equation (1) the governing equation relating $\{\Delta F\}$ and $\{\Delta U\}$ is

$$\{\Delta F\} = [K]\{\Delta U\} \tag{2}$$

To apply equation (2), consider two typical bodies A and B in contact over a surface C–C′ as depicted in figure 1. Let A and B be discretized into elements and nodes in the usual manner of finite element analysis, except that in the contact region let each node on the surface of A have a corresponding opposite, or mating, node on the surface of B (see fig. 1).

Consider a typical pair of mating, contacting nodes, i and i′, as depicted in figure 2. Let t–n be local Cartesian axes defining the "average" tangential and normal directions. Let $\{\Delta R_{jn}\}$ and $\{\Delta R_{jt}\}$ (j = a,b) represent incremental normal and tangential loadings on i and i′. Similarly, let $\{\Delta U_{jn}\}$ and $\{\Delta U_{jt}\}$ (j = a,b) be the resulting incremental displacements.

The contact status can be categorized as being either (1) open, (2) closed and sticking, or (3) closed and sliding. In each case the equilibrium and continuity conditions must be satisfied. That is,

(1) For open nodes (no contact)

$$\{\Delta U_{bn}\} - \{\Delta U_{an}\} \leq \{\delta_n\}$$

$$\{\Delta R_{an}\} = \{\Delta R_{bn}\} = \{0\} \tag{3}$$

$$\{\Delta R_{at}\} = \{\Delta R_{bt}\} = \{0\}$$

(2) For closed and sticking nodes (no relative movement)

$$\{\Delta U_{bn}\} = \{\Delta U_{an}\} + \{\delta_n\}$$

$$\{\Delta U_{at}\} = \{\Delta U_{bt}\}$$

$$\{\Delta R_{an}\} = -\{\Delta R_{bn}\} \tag{4}$$

$$\{\Delta R_{at}\} = -\{\Delta R_{bt}\}$$

(3) For closed and sliding nodes (tangential movement)

$$\{\Delta U_{bn}\} = \{\Delta U_{an}\} + \{\delta_n\}$$

$$\{\Delta R_{bn} = -\{\Delta R_{an}\} \tag{5}$$

$$\{\Delta R_{bt}\} = -\{\Delta R_{at}\} = \pm\mu\{\Delta R_{an}\}$$

where $\{\delta_n\}$ is the normal "gap" vector between contacting nodes and μ is the coefficient of friction between the surfaces. (Coulomb friction is assumed and the sign in the final terms of equation (4) is chosen so that energy is dissipated.)

To use the constraint conditions of equations (3) to (5) with the governing equations, it is useful to transform the columns and rows, which are associated with the contacting node pairs, from the global (x,y) system to the local (n,t) system. Let $\{\Delta\hat{F}\}$ and $\{\Delta\hat{U}\}$ represent the incremental load and displacement vectors in the local system, and let $[T]$ be the (orthogonal) transformation matrix from the local to the global system. Then

$$\{\Delta F\} = [T]\{\Delta\hat{F}\}$$

and (6)

$$\{\Delta U\} = [T]\{\Delta\hat{U}\}$$

By substituting equations (6) into equation (2), we obtain the relation

$$\{\Delta\hat{F}\} = [T]^T[K][T]\{\Delta\hat{U}\} = [\hat{K}]\{\Delta\hat{U}\} \tag{7}$$

where the stiffness matrix $[\hat{K}]$ is defined by inspection.

By assembling together the terms associated with the contacting nodes, equation (7) can be expressed as

$$\begin{bmatrix} \Delta F_a \\ \Delta F_{an} + \Delta R_{an} \\ \Delta F_{at} + \Delta R_{at} \\ \Delta F_{bn} + \Delta R_{bn} \\ \Delta F_{bt} + \Delta R_{bt} \\ \Delta F_b \end{bmatrix} = [\hat{K}] \begin{bmatrix} \Delta U_a \\ \Delta U_{an} \\ \Delta U_{at} \\ \Delta U_{bn} \\ \Delta U_{bt} \\ \Delta U_b \end{bmatrix} \tag{8}$$

Equation (8) is then the matrix form of the force-displacement relations. To obtain the complete set of governing equations, it is necessary to impose the contacting boundary constraints of equations (3) to (5) for the three contact conditions: open nodes (no contact), closed and sticking nodes (no relative movement), and closed and sliding nodes (tangential movement).

Open nodes (no contact).—In this case no constraints are needed. However, equations (3) need to be satisfied during each numerical iteration for which any matching node pairs are deemed to be open.

Closed and sticking nodes (no relative movement).—In this case equations (4) are constraining relations that need to be satisfied. After substitution from equations (4), equations (8) take the form

$$\begin{bmatrix} \Delta F_a \\ \Delta F_{an} + \Delta R_{an} \\ \Delta F_{at} + \Delta R_{at} \\ \Delta F_{bn} - \Delta R_{an} \\ \Delta F_{bt} - \Delta R_{at} \\ \Delta F_b \end{bmatrix} = [\hat{K}] \begin{bmatrix} \Delta U_a \\ \Delta U_{an} \\ \Delta U_{at} \\ \Delta U_{an} + \delta_n \\ \Delta U_{at} \\ \Delta U_b \end{bmatrix} \tag{9}$$

Equation (9) can be reduced by eliminating the unknown contact forces $\{\Delta R_{an}\}$ and $\{\Delta R_{at}\}$. To this end, we introduce rectangular transformation matrices $[S_1]$ and $[S_2]$ defined as

$$[S_1] = \begin{bmatrix} I_a & 0 & 0 & 0 \\ 0 & I_c & 0 & 0 \\ 0 & 0 & I_c & 0 \\ 0 & I_c & 0 & 0 \\ 0 & 0 & I_c & 0 \\ 0 & 0 & 0 & I_b \end{bmatrix} \quad \text{and} \quad [S_2] = \begin{bmatrix} 0 & 0 & 0 & 0 \\ 0 & 0 & 0 & 0 \\ 0 & 0 & 0 & 0 \\ 0 & I_c & 0 & 0 \\ 0 & 0 & 0 & 0 \\ 0 & 0 & 0 & 0 \end{bmatrix} \tag{10}$$

where I_a is an identity matrix with dimensions equal to the number of degrees of freedom of the nodes of body a less the number of degrees of freedom of the contact nodes, I_b is the corresponding identity matrix for body b, and I_c is an identity matrix with dimensions equal to the number of degrees of freedom of the contact nodes. For example, if a finite element model has 40 nodes for each of bodies a and b and if there are 5 contact node pairs, then I_a has dimensions $(40 - 5) \times 2 = 70$, I_b has dimensions $(40 - 5) \times 2 = 70$, and I_c has dimensions $5 \times 2 = 10$. Observe that these matrices have properties such that

$$\begin{bmatrix} \Delta U_a \\ \Delta U_{an} \\ \Delta U_{at} \\ \Delta U_{an} + \delta_n \\ \Delta U_{at} \\ \Delta U_{bt} \end{bmatrix} = [S_1] \begin{bmatrix} \Delta U_a \\ \Delta U_{an} \\ \Delta U_{at} \\ \Delta U_b \end{bmatrix} + [S_2] \begin{bmatrix} 0 \\ \delta_n \\ 0 \\ 0 \end{bmatrix} \tag{11}$$

and

$$\begin{bmatrix} \Delta F_a \\ \Delta F_{an} + \Delta F_{bn} \\ \Delta F_{at} + \mu \Delta F_{bt} \\ \Delta F_b \end{bmatrix} = [S_1]^T \begin{bmatrix} \Delta F_a \\ \Delta F_{an} + \Delta R_{an} \\ \Delta F_{at} + \Delta R_{at} \\ \Delta F_{bn} - \Delta R_{an} \\ \Delta F_{bt} - \Delta R_{at} \\ \Delta F_b \end{bmatrix} \tag{12}$$

Premultiplying equation (9) by $[S_1]^T$ and substituting from equation (11) gives the reduced system

$$\begin{bmatrix} \Delta F_a \\ \Delta F_{an} + \Delta F_{bn} \\ \Delta F_{at} + \Delta F_{bt} \\ \Delta F_b \end{bmatrix} - [S_1]^T[\hat{K}][S_2]\begin{bmatrix} 0 \\ \delta_n \\ 0 \\ 0 \end{bmatrix} = [S_1]^T[\hat{K}][S_1]\begin{bmatrix} \Delta U_a \\ \Delta U_{an} \\ \Delta U_{at} \\ \Delta U_b \end{bmatrix} \tag{13}$$

Closed and sliding nodes (tangential movement).—In this case equations (5) are constraining relations that need to be satisfied. After substitution from equations (5), equations (8) take the form

$$\begin{bmatrix} \Delta F_a \\ \Delta F_{an} + \Delta R_{an} \\ \Delta F_{at} \pm \mu \Delta R_{an} \\ \Delta F_{bn} - \Delta R_{an} \\ \Delta F_{bt} \mp \mu \Delta R_{an} \\ \Delta F_b \end{bmatrix} = [\hat{K}] \begin{bmatrix} \Delta U_a \\ \Delta U_{an} \\ \Delta U_{at} \\ \Delta U_{an} + \delta_n \\ \Delta U_{bt} \\ \Delta U_b \end{bmatrix} \tag{14}$$

By following a similar procedure to that of case (2), equations (14) can be reduced to the form

$$\begin{bmatrix} \Delta F_a \\ \Delta F_{an} + \Delta F_{bn} \\ \Delta F_{at} \mp \mu \Delta F_{an} \\ \Delta F_{bt} \pm \mu \Delta F_{an} \\ \Delta F_b \end{bmatrix} - [Q_3][\hat{K}][Q_2]\begin{bmatrix} 0 \\ \delta_n \\ 0 \\ 0 \end{bmatrix} = [Q_3][\hat{K}][Q_1]\begin{bmatrix} \Delta U_a \\ \Delta U_{an} \\ \Delta U_{at} \\ \Delta U_{bt} \\ \Delta U_b \end{bmatrix} \tag{15}$$

where $[Q_1]$, $[Q_2]$, and $[Q_3]$ are transformation matrices defined as

$$[Q_1] = \begin{bmatrix} I_a & 0 & 0 & 0 \\ 0 & I_c & 0 & 0 \\ 0 & I_c & 0 & 0 \\ 0 & 0 & I_c & 0 \\ 0 & 0 & 0 & I_b \end{bmatrix}, \quad [Q_2] = \begin{bmatrix} 0 & 0 & 0 & 0 \\ 0 & 0 & 0 & 0 \\ 0 & 0 & 0 & 0 \\ 0 & I_c & 0 & 0 \\ 0 & 0 & 0 & 0 \\ 0 & 0 & 0 & 0 \end{bmatrix}, \text{ and } [Q_3] = \begin{bmatrix} I_a & 0 & 0 & 0 & 0 & 0 \\ 0 & I_c & 0 & I_c & 0 & 0 \\ 0 & \mp\mu I_c & I_c & 0 & 0 & 0 \\ 0 & \pm\mu I_c & 0 & 0 & I_c & 0 \\ 0 & 0 & 0 & 0 & 0 & I_b \end{bmatrix} \tag{16}$$

Observe that in this case the stiffness matrix $[Q_3][\hat{k}][Q_1]$ is not symmetric. The dissymmetry is due to the Coulomb friction forces. The $\pm$ and $\mp$ signs are chosen to dissipate energy because the work due to friction forces is negative.

The governing equations, equations (8), (13), and (15), can be solved for the incremental displacements $\{\Delta U_{an}\}$, $\{\Delta U_{at}\}$, $\{\Delta U_b\}$, and $\{\Delta U_{bt}\}$. Then by backsubstitution the incremental forces $\{\Delta R_{an}\}$, $\{\Delta R_{at}\}$, $\{\Delta R_b\}$, and $\{\Delta R_{bt}\}$ can be obtained. However, at each incremental load the assumed contact conditions must be checked and adjusted, if necessary. Table I lists the contact region criteria and the transition boundaries. Iterations must be performed at each increment until convergence between assumed and calculated contact and frictional conditions is obtained.

AUTOMATION OF METHOD

The analysis method is based upon the assumption that the size of the load increments is sufficiently small that there is a linear load-displacement relationship and also that there is no more than one change of contact condition or phase in any load step. An algorithm to automatically limit the size of the load increment can be developed by studying the transitions between contact phases. The procedure is based upon an evaluation of the amount of load increment needed to reach a phase boundary. This "amount" is measured in terms of "scale factors."

The development proceeds as follows: First, we categorize the contact phase change as being either (1) from open to contact or (2) from contact to open. Next, within the contact region we categorize phase change as being either (3) from sticking to sliding or (4) from sliding to sticking.

From open to contact.—Suppose a load increment $\{\Delta F\}$ causes an open pair of contact nodes, say a and b, to come into contact and even pass each other (analytically). Then, due to the assumed linearity, the proportion $\alpha_1\{\Delta F\}$ of the load increment needed to exactly close the gap distance δ can be determined. Specifically, let the relative displacement of a and b in the direction n, normal to the surface, due to $\{\Delta F\}_1$ be $\Delta U_{an} - \Delta U_{bn}$. Then the scale factor α_1 needed to close the gap without penetration is determined by the relation

$$\alpha_1(\Delta U_{an} - \Delta U_{bn}) = \delta \tag{17a}$$

or

$$\alpha_1 = \delta/(\Delta U_{an} - \Delta U_{bn}) \tag{17b}$$

From contact to open.—If the normal force R_n between two contacting nodes a and b becomes a tensile force, the surfaces will separate. If ΔR_n is the normal load increment during separation, in a typical iteration step, the proportion $\alpha_2 \Delta R_n$ of the load increment needed to exactly reach the transition between contact and separation is given by the relation

$$R_n + \alpha_2 \Delta R_n = 0 \quad \text{or} \quad \alpha_2 = -R_n/\Delta R_n \tag{18}$$

where α_2 is the scale factor.

From sticking to sliding contact.—From Coulomb's law of sliding with friction there will be a transition between sticking and sliding at a contacting node pair when the tangential force R_t exceeds μR_n, where μ is the friction coefficient and where, as before, R_n is the normal force. Let ΔR_t and ΔR_n be increments in the tangential and normal contact forces due to a load increment $\{\Delta F\}$. If the load increment is sufficiently small, ΔR_t and ΔR_n are proportional to the magnitude of $\{\Delta F\}$ and hence proportional to each other. Then the proportions $\alpha_3 \Delta R_t$ and $\alpha_3 \Delta R_n$ of the tangential and normal force increments needed to reach the transition between sticking and sliding are given by the expression

$$\pm(R_t + \alpha_3 \Delta R_t) = \mu(R_n + \alpha_3 \Delta R_n) \tag{19}$$

where the sign is positive if $R_t \Delta R_n \leq R_n \Delta R_t$ and negative otherwise. Hence, the scale factor α_3 is

$$\alpha_3 = -\frac{R_t - \mu \Delta R_n}{\Delta R_t - \mu \Delta R_n} \qquad \text{for} \qquad R_t \Delta R_n \leq R_n \Delta R_t \tag{20}$$

and

$$\alpha_3 = -\frac{R_t + \mu \Delta R_n}{\Delta R_t + \mu \Delta R_n} \qquad \text{for} \qquad R_t \Delta R_n > R_n \Delta R_t \tag{21}$$

Note that the static (stick condition) friction coefficient is generally slightly higher than the dynamic (sliding) friction coefficient. This difference has been neglected in this analysis.

From sliding to stick contact.—It is difficult to establish and calculate a load scale factor for the transition from sliding to sticking contact. Therefore, for this case we simply assume all sliding nodes are sticking as a new load increment is applied. Then, we examine the sliding/sticking character of the contacting nodes: If they are sliding, no status change has occurred. However, if they are sticking (indicating a status change), the load increment must be reduced to establish the location and loading of the phase change.

After the scale factors $\alpha_1, \alpha_2, \alpha_3$ are determined for each case, for all contacting node pairs, the minimum of these (designated α) is selected as the global load scale factor. That is, the load increment $\{\Delta F\}$ is reduced to $\alpha\{\Delta F\}$ and the process is repeated.

When friction is present and where there is a tentative phase change from sticking to sliding, the accuracy of the incremental procedure can be improved by monitoring the friction forces R_t. Specifically, sliding will occur when R_t approaches μR_n. Hence, an additional iteration criterion can be established by requiring R_t to satisfy the relation

$$(1 - e)\mu R_n < R_t < \mu R_n \qquad (0 < e \leq 1) \tag{22}$$

where e is an accuracy parameter.

Figure 3 shows a flow chart outlining the steps of the procedure.

VALIDATION: CONTACT BETWEEN IDENTICAL INFINITE CYLINDERS

A computer code was written to execute the foregoing algorithm. To validate the algorithm and the code, we first considered the contact between two semicylinders as depicted in figure 4. The semicylinders are geometrically identical, but they were given different elastic properties to investigate and illustrate the effect of elasticity upon the contact mechanics. They each have radius $R_a = R_b = 1.0$ inch and infinite length. Their elastic moduli and Poisson ratios are

$$\begin{aligned} E_a &= 3.0\times10^7 \text{ psi} \qquad \text{(steel)} \\ E_b &= 1.8\times10^7 \text{ psi} \qquad \text{(beryllium copper)} \\ \nu_a &= 0.292 \\ \nu_b &= 0.285 \end{aligned} \tag{23}$$

The cylinders were aligned with parallel axes and pressed together by a uniform distributed load p of 5×10^3 psi, as depicted in figure 4. Figure 5 shows the finite element mesh for the semicylinders. The mesh is very fine in the contact region. It has a total of 412 nodes and 364 linear quadrilateral plane strain elements. Three contact conditions were examined: Frictionless contact, friction contact without sliding, and friction contact with sliding.

Frictionless contact.—Figure 6 shows the resulting stress distribution for frictionless contact. The horizontal and vertical normal stresses and the maximum shear stresses are plotted along the vertical axis of symmetry. The stresses are measured in multiples of the maximum normal contact pressure p_0 of the Hertz theory. Comparisons with the classical Hertz solution (ref. 9) are also given.

Figure 7 shows the distribution of normal stress in the contact area and also a comparison with the Hertz solution, where a is the semilength of contact of the Hertz solution. The contact area determined by the finite element solution is approximate in that the boundary between the contact and open regions lies between the closed and open node pairs. The boundary position can be estimated by interpretation.

Table II presents a comparison of the numerical results and the Hertz results for the maximum contact pressure, the maximum shear stress, and the semilength of the contact.

Friction contact without sliding.—To determine the effects of friction, the stresses were calculated with friction coefficients μ of 0.0, 0.06, 0.12, and ∞. Figure 8 shows the results for the contact forces on the upper and lower cylinders. Figure 9 shows detailed representations for portions of the normal and tangential contact forces. Observe in figure 9(a) that the maximum normal contact forces increase with the friction coefficient. However, there is relatively little increase once the coefficient exceeds 0.12. Observe also that the normal contact forces decrease slightly in the edge region when the friction coefficient increases.

Finally, table III shows the results for the semilength of the contact. As expected, the length decreases as the friction coefficient increases.

Friction contact with sliding.—To determine the effect of friction when there is slipping or sliding between contacting nodes, let the upper cylinder of figure 4 rotate counterclockwise relative to the lower cylinder. Figures 10 and 11 show the resulting maximum compressive (principal) stresses and maximum shear stresses on the upper cylinder in the contact area for various friction coefficients. Analogous and similar results were obtained for the lower cylinder.

CONTACT STRESSES BETWEEN SPUR GEAR TEETH

Consider a pair of identical spur gear teeth in contact with each other at their pitch points. Let the teeth be modeled as in figure 12 with the tooth on the right being the driving tooth. Let the teeth have a fillet radius of 0.045 inch, a face width of 0.25 inch, and a pressure angle of 20°. Let the teeth be elements of gears with a diametrical pitch of 8.0 and with 28 teeth per gear. Let the elastic modulus be 30×10^6 psi with a Poisson's ratio of 0.3. Let the driving gear have a clockwise torque of 50 000 in.-lb.

The stresses were calculated for the same friction cases as before.

Frictionless contact.—Figure 13 shows stress contour results for the maximum compressive (principal) stresses and for the maximum shear stresses. The maximum contact pressure was found to be 8.11×10^5 psi, which is approximately 10 percent higher than that predicted by the Hertz method (ref. 10):

Friction contact without sliding.—Figure 14 shows the distribution of normal and tangential contact forces for the driving gear for four friction coefficients: 0, 0.05, 0.10, and ∞. Analogous results were obtained for the driven gear.

Friction contact with sliding.—Figure 15 shows the maximum compressive (principal) stress and maximum shear stress distributions in the contact region for the driving gear tooth. Analogous results were obtained for the driven gear.

DISCUSSION

The results demonstrate the feasibility and the practicality of using the finite element method for gear stress calculations. Success in obtaining reliable results, however, is dependent upon the incrementation of the load to establish the extent of the contact area, which is unknown at the start of the problem.

Because the contact region boundaries are unknown, they must be determined iteratively. These boundaries are more sensitive to the loading than are the stresses. This is seen in table II, where the difference in the stresses between the Hertz and finite element analyses is much less than the difference in

the contact region. The sensitivity of the contact region arises from the near-parallel surfaces of the contacting bodies in the contact region.

The inclusion of friction effects creates an additional complexity in the analysis. Indeed, friction produces a dissymmetry in the stiffness matrix that significantly increases the computational effort. The computational effort was reduced by treating the friction forces as known external tangential forces that are determined from the previous iteration step.

The results also show that friction produces higher stress in the contact region than when friction is absent. This means that precise surface geometry, polished surfaces, and lubrication can significantly reduce the stresses and thus increase surface life.

The gear stress analysis is not comprehensive but only representative and illustrative of spur gear tooth stresses. The analysis is conducted for pitch point contact where there is no sliding due to gear kinematics. This means that an assumption of frictionless contact at the pitch point is very reasonable. Indeed, figures 14 and 15 show that friction has a relatively small effect on the analysis.

Plane strain finite elements were used for the analysis presented in this paper. Plane strain is most suitable for very thick bodies such as the infinitely long cylinders used to compare the analysis with Hertz theory. For gear teeth, plane stress finite elements may be more appropriate, especially for narrow-face-width gears. Finally, the analysis assumes either static or sliding contact, whereas the contact between gear teeth in service is divided between sliding and rolling phases. Hence, more study is needed to obtain a comprehensive stress analysis.

CONCLUDING REMARKS

An incremental finite element procedure has been investigated for the analysis of contact stresses with application to meshing spur gears. The following conclusions have been reached:

1. The feasibility and practicality of the procedure were established through several examples and by favorable comparison of results with those of the classical Hertz method.

2. Because the contact area is not known a priori, it was necessary to employ an iterative procedure (herein called the load incremental procedure) to simultaneously determine the stresses and the contact area.

3. The presence of friction between contacting surfaces increases the contact stress. This in turn means that precise surface geometry, polished surfaces, and effective lubrication can reduce contact stresses and thus increase surface life.

4. The method is directly applicable to gear stress calculations. However, more analyses are needed to obtain a comprehensive understanding of contact mechanics throughout a mesh cycle.

REFERENCES

1. Chang, S.H.; Huston, R.L.; and Coy, J.J.: A Finite Element Stress Analysis of Spur Gears Including Fillet Radii and Rim Thickness Effects. J. Mechanisms Transmissions Automation Des., vol. 105, no. 3, 1983, pp. 327–330.

2. Oda, S.; Nagamura, K.; and Aoki, K.: Stress Analysis of Thin Rim Spur Gears by Finite Element Method. Bull. JSME, vol. 24, no. 193, 1981, pp. 1273–1280.

3. Wilson, E.A.; and Parsons, B.: Finite Element Analysis of Elastic Contact Problems Using Differential Displacements. Int. J. Numer. Methods. Eng., vol. 2, 1970, pp. 387–395.

4. Ohte, S.: Finite Element Analysis of Elastic Contact Problems. Bull. JSME, vol. 16, no. 95, May 1973, pp. 797–804.

5. Okamoto, N.: and Nakazawa, M.: Finite Element Incremental Contact Analysis With Various Frictional Conditions. Int. J. Numer. Methods. Eng., vol. 14, no. 3, 1979, pp. 337–357.

6. Skinner, R.N.; and Streiner, P.: ASKA–CA Analysis of Linear Contact Problems UM229. Institut für Statik und Dynamik, University of Stuttgart, Stuttgart, 1979.

7. Urzua, J.L., et al.: Analysis Procedure for Frictional Contact Problems Using Interface Finite Elements. Structural Res. Series No. 438, University of Illinois, Mar. 1977.

8. Torstenfelt, B.R.: An Automatic Incrementation Technique for Contact Problems With Friction. Comput. Struct., vol. 19, no. 3, 1984, pp. 393–400.

9. Johnson, K.L.: Contact Mechanics. Cambridge University Press, 1985.

10. Colbourne, J.R.: The Geometry of Involute Gears. Springer-Verlag, 1987.

TABLE I.—CONTACT CRITERIA AND TRANSITION BOUNDARIES

Condition		Criterion
Before	After	
Open	Open	$(\Delta U_{bn} - \Delta U_{an}) - \delta_n > 0$
	Close	$(\Delta U_{bn} - \Delta U_{an}) - \delta_n \leq 0$
Stick	Stick	$R_{an} \geq 0, \lvert R_{at}\rvert < \mu\lvert R_{an}\rvert$
	Open	$R_{an} < 0$
	Sliding	$R_{an} \geq 0, \lvert R_{at}\rvert \geq \mu\lvert R_{an}\rvert$
Sliding	Stick	$R_{an} \geq 0, \Delta R_{at}(\Delta U_{at} - \Delta U_{bt}) > 0$
	Open	$R_{an} < 0$
	Sliding	$R_{an} \geq 0, \Delta R_{at}(\Delta U_{at} - \Delta U_{bt}) \leq 0$

TABLE II.—COMPARISON OF RESULTS OF FEM AND HERTZ

	FEM	Hertz method	Error, percent
Maximum contact pressure, p_0, ksi	19.33	19.76	−2.20
Maximum shear stress, τ_{max}, ksi	5.536	5.928	−2.60
Semilength of contact, a, in.	.01732	.01611	7.51

TABLE III.—FRICTION COEFFICIENT AND SEMILENGTH OF CONTACT

Friction coefficient, μ	Semilength of contact, a, in.
0	0.01732
.06	.01730
.12	.01729
∞	.01727

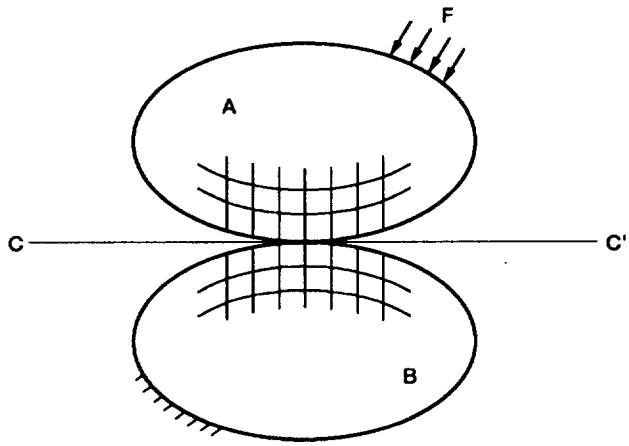

Figure 1.—Two typical bodies in contact.

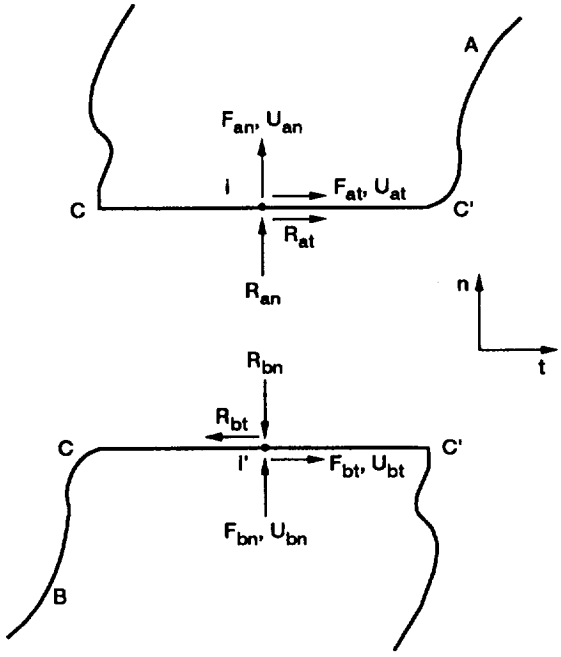

Figure 2.—Pairs of typical contact forces.

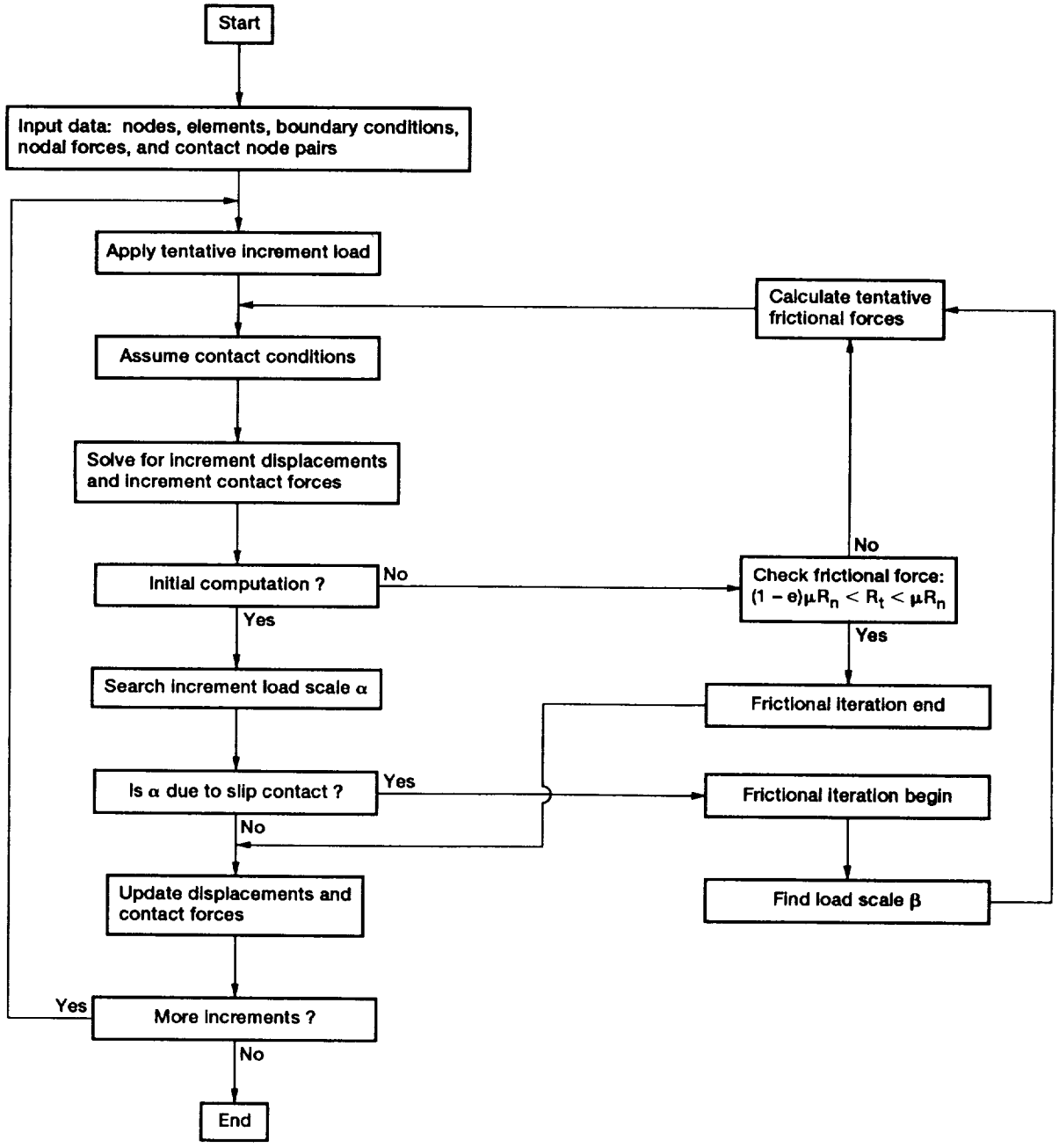

Figure 3.—Flow chart for load incrementation iteration.

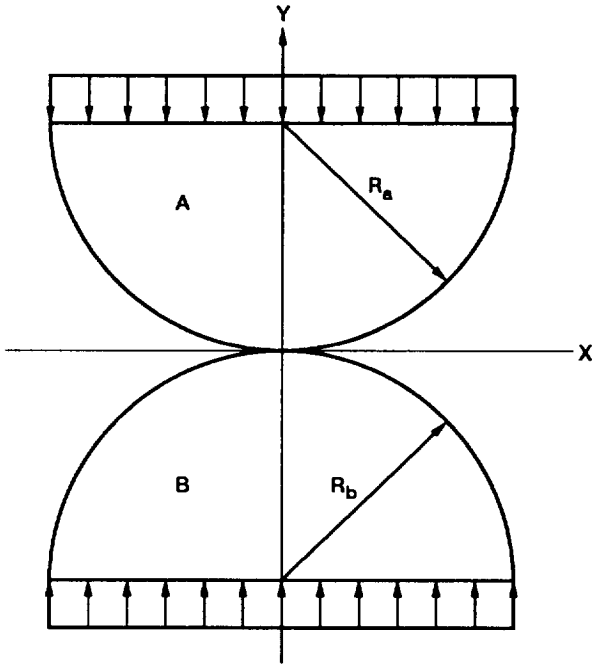

Figure 4.—Contact between two semicylinders.

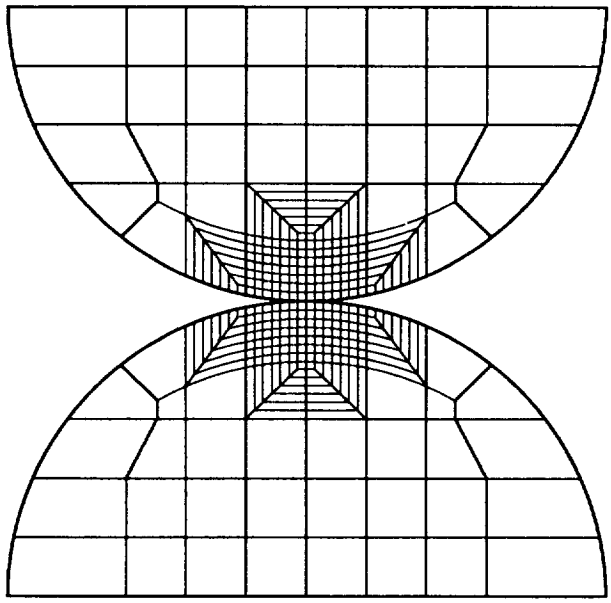

Figure 5.—Semicylinder finite element mesh.

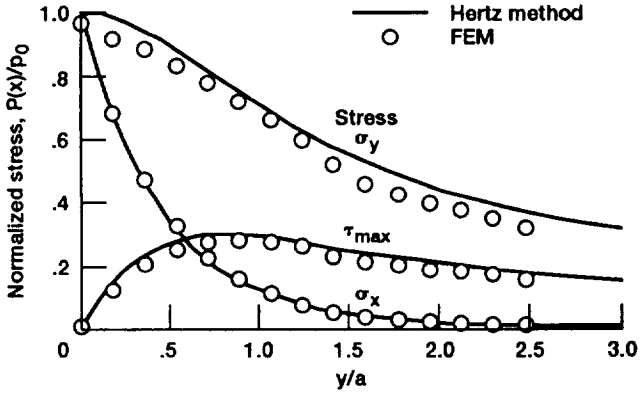

Figure 6.—Subsurface stresses along axis of symmetry. (Stress values are normalized by p_0, the maximum normal contact pressure.)

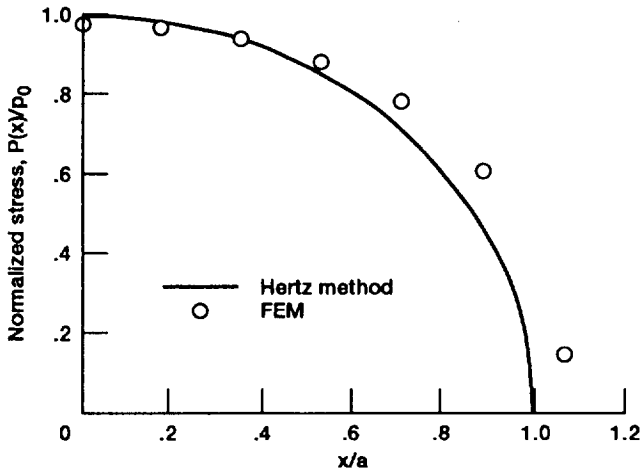

Figure 7.—Distribution of normal stress in contact surface. (Stress values are normalized by p_0, the maximum normal contact pressure.)

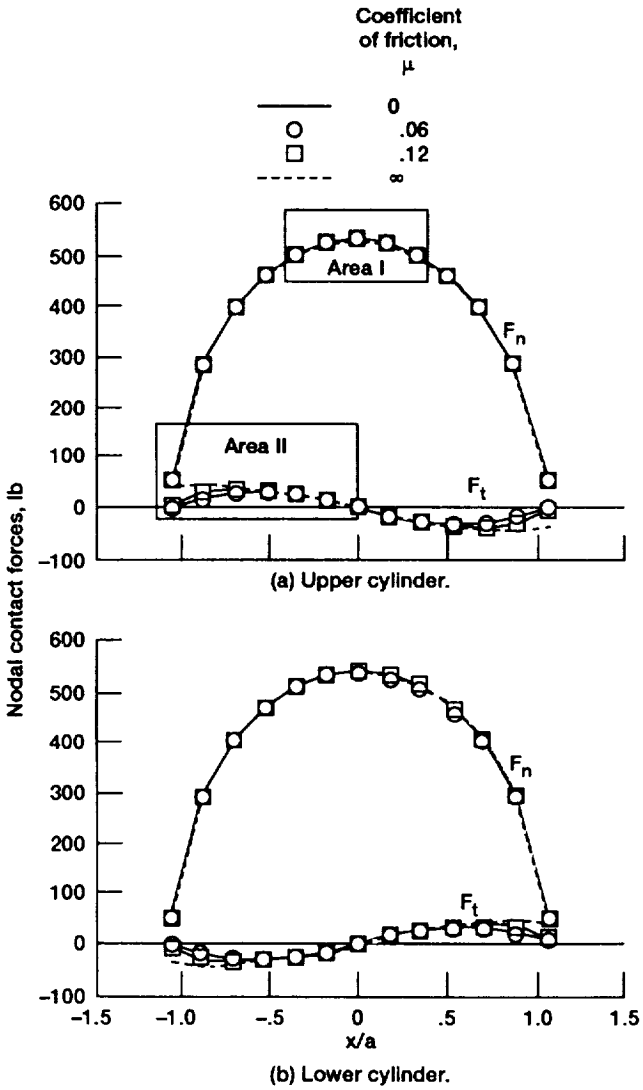

(a) Upper cylinder.

(b) Lower cylinder.

Figure 8.—Distribution of contact forces.

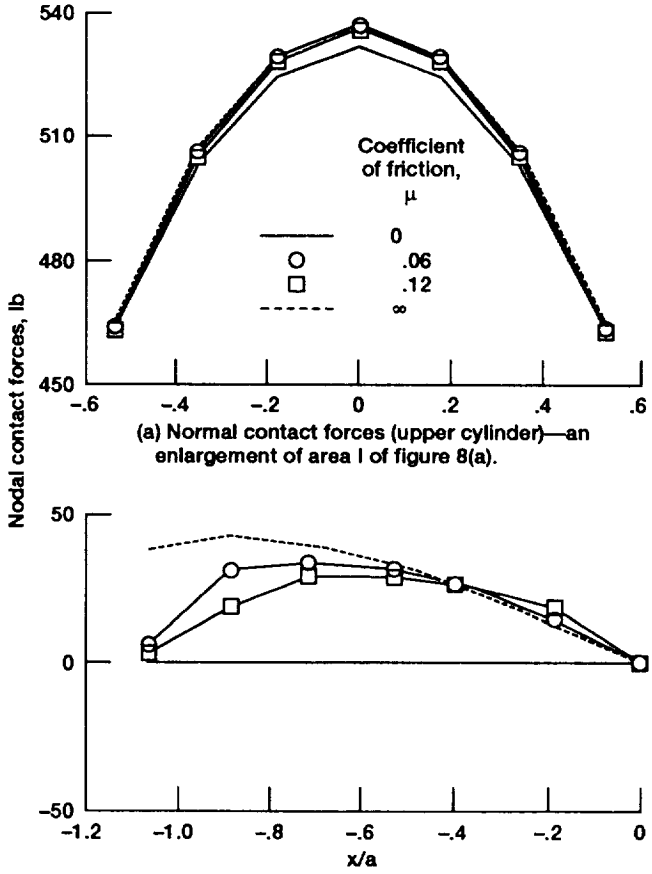

(a) Normal contact forces (upper cylinder)—an enlargement of area I of figure 8(a).

(b) Tangential contact forces (upper cylinder)—an enlargement of area II of figure 8(a).

Figure 9.—Detailed representation of forces.

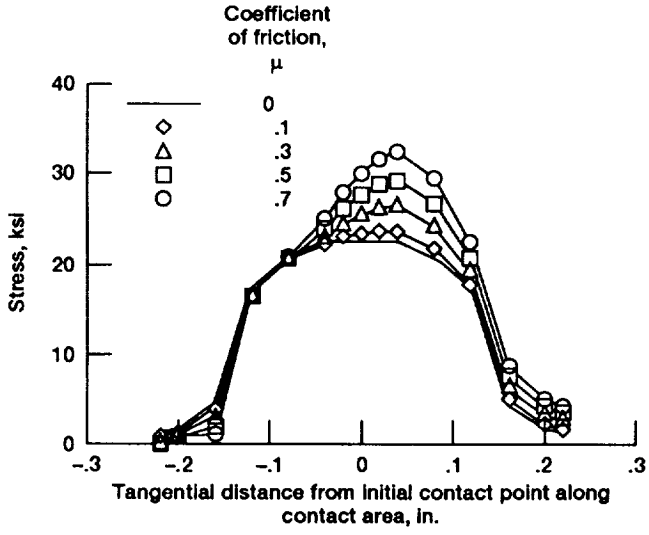

Figure 10.—Maximum compressive (principal) stresses on contact surface of upper cylinder (sliding case).

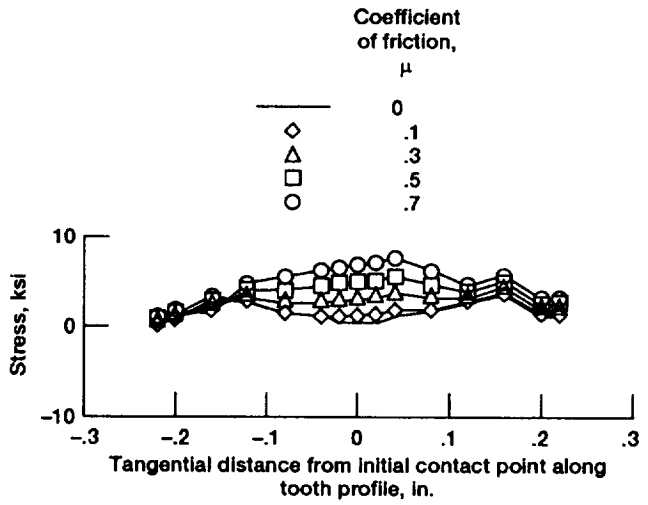

Figure 11.—Maximum shear stresses on upper cylinder in contact area (sliding case).

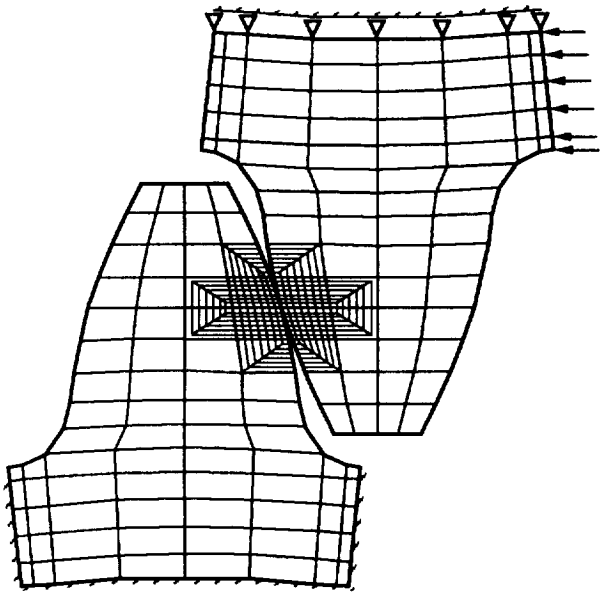

Figure 12.—Spur gear teeth in contact at pitch point.

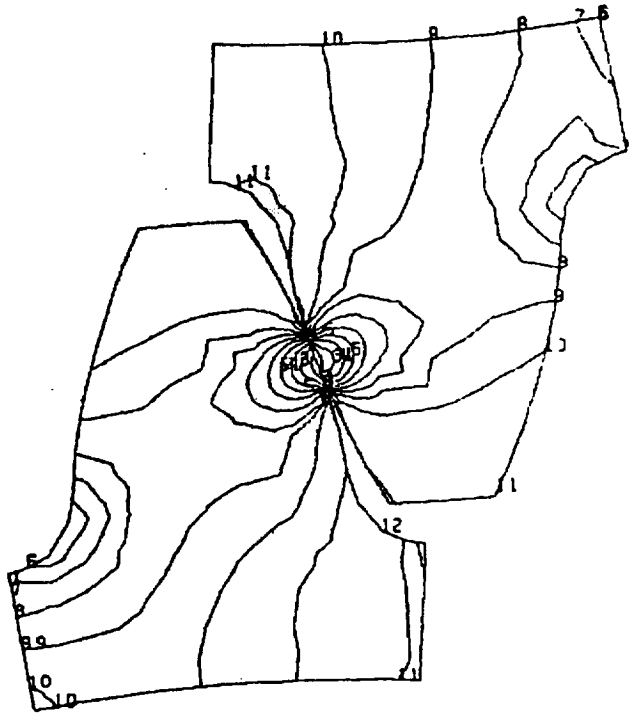

(a) Maximum compressive (principal) stress.

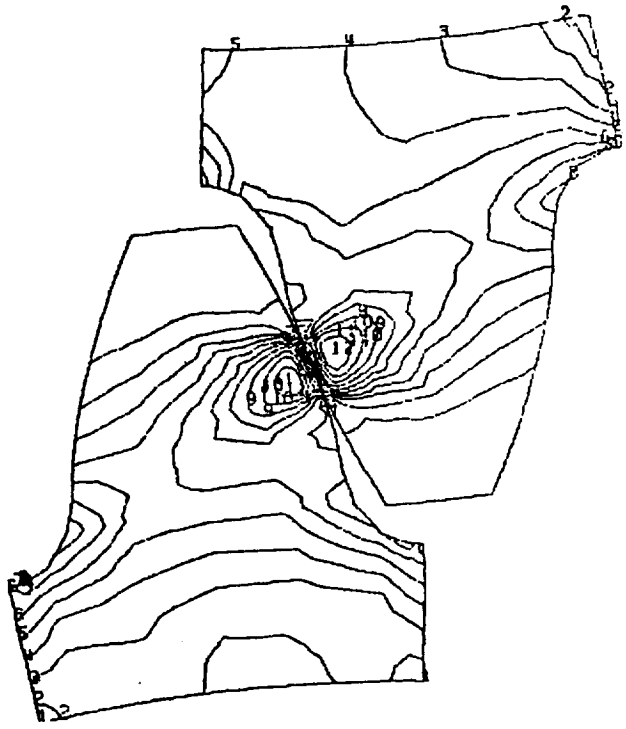

(b) Maximum shear stress.

Figure 13.—Stress contours for frictionless contact.

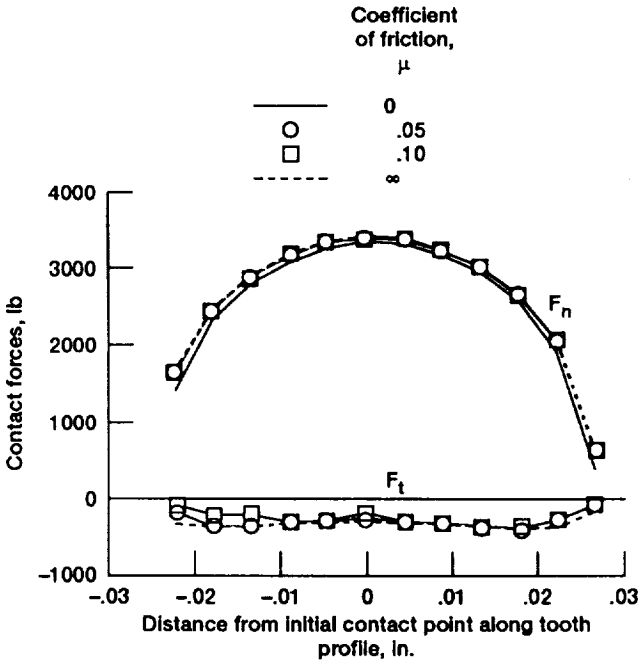

Figure 14.—Distribution of contact forces on driving gear.

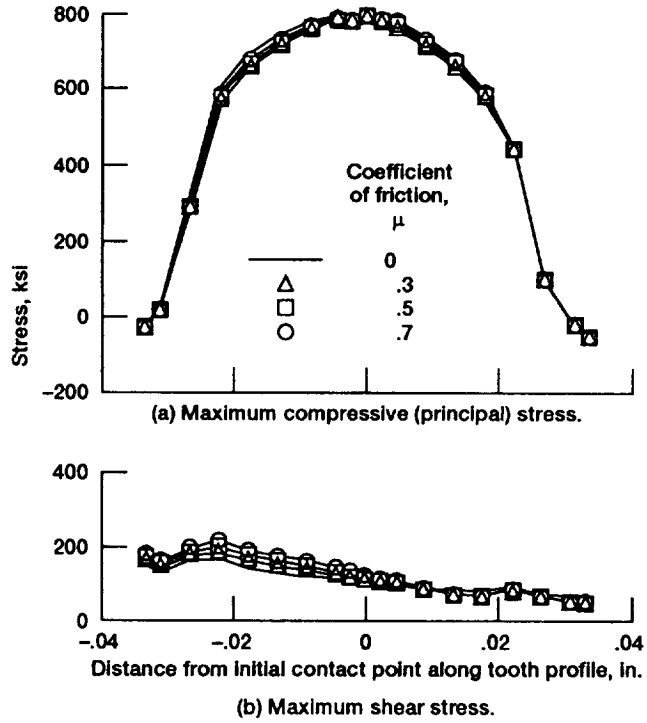

Figure 15.—Stresses on driving gear teeth.

REPORT DOCUMENTATION PAGE

Form Approved
OMB No. 0704-0188

1. AGENCY USE ONLY (Leave blank)	2. REPORT DATE	3. REPORT TYPE AND DATES COVERED
	March 1992	Technical Memorandum

4. TITLE AND SUBTITLE

Contact Stresses in Meshing Spur Gear Teeth: Use of an Incremental Finite Element Procedure

5. FUNDING NUMBERS

WU-505-63-36
1L162211A47A

6. AUTHOR(S)

Chih-Ming Hsieh, Ronald L. Huston, and Fred B. Oswald

7. PERFORMING ORGANIZATION NAME(S) AND ADDRESS(ES)

NASA Lewis Research Center
Cleveland, Ohio 44135-3191
and
Propulsion Directorate
U.S. Army Aviation Systems Command
Cleveland, Ohio 44135-3191

8. PERFORMING ORGANIZATION REPORT NUMBER

E-6776

9. SPONSORING/MONITORING AGENCY NAMES(S) AND ADDRESS(ES)

National Aeronautics and Space Administration
Washington, D.C. 20546-0001
and
U.S. Army Aviation Systems Command
St. Louis, Mo. 63120-1798

10. SPONSORING/MONITORING AGENCY REPORT NUMBER

NASA TM-105388
AVSCOM TR-90-C-029

11. SUPPLEMENTARY NOTES

Chih-Ming Hsieh and Ronald L. Huston, Department of Mechanical, Industrial, and Nuclear Engineering, University of Cincinnati, Cincinnati, Ohio 45221-0072 (work funded under NASA Grant NSG3-188). Fred B. Oswald, NASA Lewis Research Center. Responsible person, Fred B. Oswald, (216) 433-3957.

12a. DISTRIBUTION/AVAILABILITY STATEMENT

Unclassified - Unlimited
Subject Category 37

12b. DISTRIBUTION CODE

13. ABSTRACT *(Maximum 200 words)*

Contact stresses in meshing spur gear teeth are examined. The analysis is based upon an incremental finite element procedure that simultaneously determines the stresses in and the contact region between the meshing teeth. The teeth themselves are modeled by two-dimensional plane strain elements. Friction effects are included, with the friction forces assumed to obey Coulomb's law. The analysis also assumes that the displacements are small and that the tooth materials are linearly elastic. The analysis procedure is validated by comparing its results with those for the classical two contacting semicylinders obtained from the Hertz method. Agreement is excellent.

14. SUBJECT TERMS

Contact stress; Finite element; Spur gears; Friction

15. NUMBER OF PAGES

22

16. PRICE CODE

A03

17. SECURITY CLASSIFICATION OF REPORT	18. SECURITY CLASSIFICATION OF THIS PAGE	19. SECURITY CLASSIFICATION OF ABSTRACT	20. LIMITATION OF ABSTRACT
Unclassified	Unclassified	Unclassified	